ORIGINAL ARTICLE

Recognizing knee pathologies by classifying instantaneous screws of the six degrees-of-freedom knee motion

Alon Wolf · Amir Degani

Abstract We address the problem of knee pathology assessment by using screw theory to describe the knee motion and by using the screw representation of the motion as an input to a machine learning classifier. The flexions of knees with different pathologies are tracked using an optical tracking system. The instantaneous screw parameters which describe the transformation of the tibia with respect to the femur in each two successive observation is represented as the instantaneous screw axis of the motion given in its *Plücker* line coordinates along with its corresponding pitch. The set of instantaneous screw parameters associated with a particular knee with a given pathology is then identified and clustered in R^6 to form a ''signature'' of the motion for the given pathology. Sawbones model and two cadaver knees with different pathologies were tracked, and the resulting screws were used to train a classifier system. The system was then tested successfully with new, never-trained-before data. The classifier demonstrated a very high success rate in identifying the knee pathology.

Keywords Knee kinematics · Screw axis · Pathology classification · Support vector machines

A. Wolf (✉)
Faculty of Mechanical Engineering, Technion,
Israel Institute of Technology,
Technion City, Haifa 32000, Israel
e-mail: alonw@tx.technion.ac.il

A. Degani
The Robotics Institute, Carnegie Mellon University,
Pittsburgh, PA 15213, USA
e-mail: degani@cmu.edu

1 Introduction

Assessment of joint pathology is not always trivial and requires, in most cases, a combination of visualization data with physical subjective tests performed by the physician. Diagnosis is particularly complex for the knee joint due to its complex structure and six degrees of freedom (DOF) motion. For example, in order to assess anterior cruciate ligament (ACL) deficient knees, there are currently three main tests that can be performed by physicians: Lachman test, pivot shift test and the anterior drawer test [20]. All of these tests are subjective and are performed manually by the physician while manipulating the patient lower limb. In our study, we demonstrate a method for which kinematic measurements of the knee are used to automatically identify knee pathologies.

Several studies have been dedicated to three-dimensional (3D) anatomically based knee models (e.g. [7, 11], etc.). In order to describe the 6-DOF motion of the knee, several studies have used the helical axis method, known also as screw motion [4, 5, 10, 12, 16, 21, 22, 25]. Screw motion was also used for study of other joints such as pelvis [14]. We also use screw coordinates to represent knee motion, and use this data to train a machine learning classifier that is later capable of identifying knee pathologies. Researchers have used classifiers in order to identify knee deficiencies. Andriacchi et al. [1] studied the anterior–posterior linear motion of the femur with respect to the tibia during gait cycle. The experimental data was presented by a one-dimensional curve correlating flexion angle to anterior–posterior displacement. This curve was later used to assess the dynamic anterior–posterior motion of the knee in the patient with ACL deficient pathology who did not develop the neuromuscular adaptation [13]. Machine learning methods were also used to classify changes in gait

characteristics of elderly non-fallers [17]. This research particularly shows that some foot placement gait measures (e.g., step width and stride variability) displayed greater associations with fall prediction. In [3] the researchers used support vector machines (SVM) classifier in order to form an automatic recognition of gait changes, due to ageing, using three types of gait measures: walking velocities and foot-ground reaction forces in the vertical and anterior–posterior directions. Test results indicated an overall accuracy of 91.7% by the SVM classifier in its capacity to distinguish the two gait patterns.

In our proposed method we incorporate all six DOF of the knee motion and represent it as a set of instantaneous screw parameters (ISP), which are then used to classify knee motion. For that, we track knee flexion by using an optical tracking system. The information provided is composed of multiple frames of relative bone states. We then calculate ISP that describe the momentary transformation between each two successive frames. We show that a set of ISP that describes a given knee motion forms a variety of points or a cluster. Moreover, we show that knees with similar classes (e.g. healthy or ACL/PCL deficient) share similar clusters. Finally, we hypothesize that once a large data set of different knees with different pathologies is created and classified (using supervised learning techniques), the kinematics of an untrained knee can be associated with one or more of the clusters reflecting on its pathology.

2 Methods

2.1 Representation of screw motion (twist)

Any given displacement of a rigid body can be effected by a rotation about an axis combined with a translation parallel to that axis [2]. This way of defining rigid body displacements is termed finite screw displacement or a twist [8]. Mathematically, the motion finite transformation can be described as a combination of a translation, d, parallel to a fixed axis A in space, and a rotation ϕ about the same axis (Fig. 1). The ratio of the translation to the rotation components is known as the *pitch* of the screw, p, and is given as

$$p = \frac{d}{\phi}. \tag{1}$$

The six parameters of the screw $ are

$$\$ = \begin{bmatrix} s \\ s_0 \times s + ps \end{bmatrix} = [L \quad M \quad N \quad P^* \quad Q^* \quad R^*]^{\mathrm{T}} \tag{2}$$

where s, is a unit vector along the screw axis direction, s_0 is a position vector of a point on A, and p is the pitch in

Eq. (1). Two extreme examples are pure rotation, $p = 0$, (Eq. 3) and pure translation, $p = \infty$, (Eq. 4):

$$\$ = \begin{bmatrix} s \\ s_0 \times s \end{bmatrix}. \tag{3}$$

$$\$ = \begin{bmatrix} 0 \\ s \end{bmatrix}. \tag{4}$$

We refer the reader to [15, 19] for a deeper discussion on screw motion of rigid bodies.

2.2 Calculating the ISP of a finite motion

Calculating the ISP of a rigid body undergoing a motion is not intuitive. Few methods have been presented in the literature regarding this issue. However, all methods provide the instantaneous screw axis parameters ($), and its corresponding pitch (p) given two finite configuration of a rigid body. In this work the algorithm presented in Davidson has been used (8, Sect. 4.6.4). Since this algorithm is long and is not the scope of this report we refer the reader to that book for a full description of the algorithm.

2.3 Cluster analysis of the screw parameters

In this work we use the SVM technique as described in [23, 24]. Generally speaking, the SVM algorithm creates a hyperplane that separates the data into classes with the maximum margin (Fig. 2). Given training examples labeled either ''yes'' or ''no'', a maximum margin hyperplane splits the ''yes'' and ''no'' training examples, such that the distance from the closest examples (the margin) to the hyperplane is maximized. To be more precise, suppose we have a data set

$$\{\mathbf{x}_i, y_i\}, \ i = 1, 2, \ldots, l, \ y_i \in \{-1, +1\}, \ \mathbf{x}_i \in \mathbb{R}. \tag{5}$$

We want to find a hyperplane which separates the positive from the negative data points; this is the ''separating hyperplane''. The points $\mathbf{x}$ which lie on the hyperplane satisfy $\mathbf{w} \cdot \mathbf{x} + b = 0$ where $\mathbf{w}$ is normal to the hyperplane, $|b|/\|\mathbf{w}\|$ is the perpendicular distance from the hyperplane to the origin, and $\|\mathbf{w}\|$ is the Euclidean norm of $\mathbf{w}$.

If the data is linearly separable then the SVM algorithm simply looks for the separating hyperplane with the largest margin, we can find this hyperplane by minimizing

$$\frac{1}{2}(\mathbf{w} \cdot \mathbf{w}) \tag{6}$$

under the constraints of

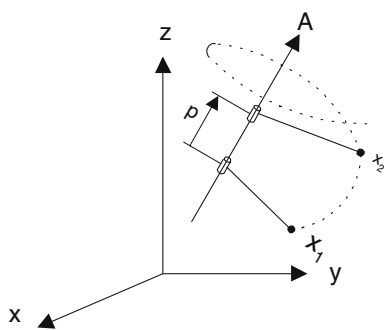$$y_i(\mathbf{x}_i \cdot \mathbf{w} + b) - 1 \geq 0 \quad \text{for all } i\text{'s}. \tag{7}$$
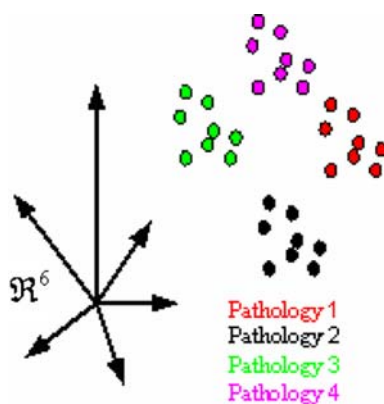
Fig. 1 Screw motion (Helical motion)

Fig. 2 Different clusters correlating to different path/set of screws

In the usual case of SVM analysis the data is first transformed into a higher-dimensional space by means of a kernel function (e.g. Gaussian Radial Basis Function—RBF) and then the hyperplane with the maximal margin is found.

If the data is not linearly separable, the modified version can be introduced as an optimization problem with a cost function for misclassification

$$\min \frac{1}{2}(\mathbf{w} \bullet \mathbf{w}) + C \sum_{i=1}^{l} \xi_i \qquad (8)$$

under the constraints of

$$y_i(\mathbf{x}_i \cdot \mathbf{w} + b) \geq 1 - \xi_i \quad \text{for all } i\text{'s}, \qquad (9)$$

where ξ_i are slack variables and the C constant is a trade-off between maximizing the width of the margin and minimizing slack variables. Non-zero ξ_i will indicate a misclassified data point.

Once classified and trained the classifier can classify new data with a class reflecting on the pathology of the source of the data which is associated with the class (Fig. 3). For a detailed overview of the SVM classifier we refer the reader to Burges [6] (Fig. 4).

3 Experimental settings

3.1 Sawbones experiment

For our first experiment we used Sawbones model of the femur and tibia. The two bones were connected by four rubber tubes to simulate the lateral collateral ligament (LCL), medial collateral ligament (MCL), posterior cruciate ligament (PCL), and the anterior cruciate ligament (ACL). It is worth noting that the mechanical properties of the actual ligaments are very different from those of the rubber tubes; however, we believe that this experimental setting provides a simplified first test for the validation of the suggested method (note that the patella is also not included for the same reason). During the experiment, optical trackers were attached to both bones (Fig. 5), and were tracked using the Polaris® system by NDI (Fig. 6). During the experiment settings, tibia was quasistatically manipulated from flexion to full extension by pulling the bone with a long (approximately 2 m) wire connected as close as possible to the center of the tibia bone, while keeping the wire within the sagittal plane of the tibia as much as possible. As opposed to a physician manipulating the tibia while grasping it, the manipulation of the tibia with the long wire imposes minimal constraints on the motion, and may provide more information on the kinematics of the
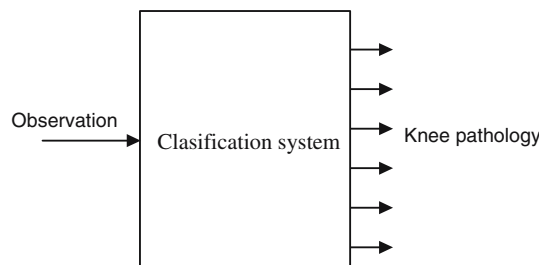

Fig. 3 AI system to identify knee pathology

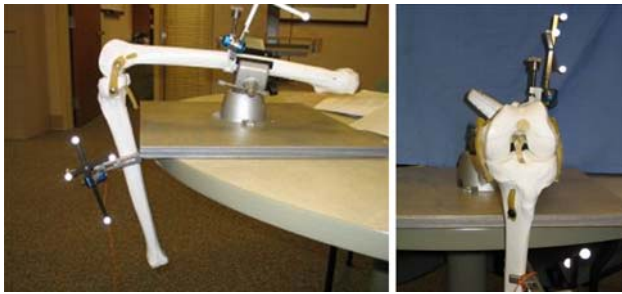**Fig. 4** Knee model with Sawbones and artificial ligaments

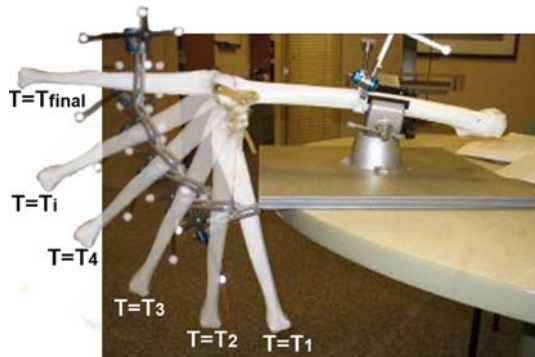**Fig. 5** Experimental setup with optical trackers attached (Sawbones)

Fig. 6 Observation while flexing the knee (Sawbones)

knee. For each manipulation from flexion to full extension approximately 300 observations are taken. This number depends on the speed that the tibia is manipulated.

For the training of the classifier we used five classes: healthy knee model and four different pathologies—ruptured ACL, ruptured LCL, ruptured MCL, and a combination of a ruptured MCL and ruptured ACL. Thirty runs were used for training, and 30 additional runs were used for testing.

3.2 Cadaver experiment

Following the Sawbones experiment, we ran a set of identical tests on two cadaver right knees (Fig. 7). Both knees included the patella. Similar to the Sawbones experiment, the tibia tracker positions were recorded in the femur tracker reference frame. Focusing on the cruciate ligaments, three classes were recorded, i.e. healthy knee, ACL deficient knee, and a combined ACL, PCL deficient knee.

For each of the classes 20 runs were recorded while quasistatically pulling the leg with a string attached to it. For training the SVM classifier, half of the observations were used, whereas the other halves were used for testing. Moreover, in order to confirm that our method is not sensitive to sampling frequency (i.e. number of points per unit of time) we created several testing sets of screws by sampling the ISP at different sampling frequencies (twice and four times the original frequency). This process of the experiment is important since it is very hard to control and synchronize the sampling frequency of the data and velocity of the knee flexion per patient.

3.3 Registration of anatomical reference frames

Although the screw representation of a motion is invariant in the same reference frame, it is still dependent on the global reference system in which it is described. Without a proper definition of a global reference system between patients, the resulting screws will differ, though still describing the same motion. For this purpose we use the anatomical reference frame (ARF) of both tibia and femur as our global system among patients. In the tibia ARF, the z-axis lies along the mechanical axis[1] (for a left knee the proximal is the positive direction and for a right knee the distal is the positive direction.) The transverse axis orthogonal to the mechanical axis serves as the x-axis where the medial direction is the positive direction for both knees. Finally, the y-axis is the axis orthogonal to both axes, where the anterior direction is the positive direction. The coordinate system is centered at the tibial knee center point (Fig. 8). As for the femur ARF, the z-axis also lies along the mechanical axis (proximal is positive for a left knee, distal positive for a right knee), the transverse axis orthogonal to the mechanical axis serves as the x-axis (medial is always positive), and the orthogonal axis to the two serves as the y-axis (anterior is always positive). The femoral ARF is also centered at the femoral knee center point (Fig. 8).

For the reported experiment we attached optical trackers both to the tibia and the femur. Then, while the trackers are still attached, both bones were scanned by CT. This procedure allows performing registration between the CT coordinate system and the other coordinate systems as can be seen in Fig. 9. Next, the following transformations were obtained from the CT scans using the HipNav[TM] system[2] [9]:

$^{CT}T_{FA}$ Femoral ARF to CT reference-frame
$^{CT}T_{TA}$ Tibial ARF to CT reference-frame
$^{TT}T_{CT}$ CT reference-frame to tibia tracker reference-frame
$^{FT}T_{CT}$ CT reference-frame to femur tracker reference-frame.

---

[1] For femur: mechanical axis refers to the line drawn from the center of the femoral head to the medial tibial spine; for tibia: mechanical axis refers to the angle formed by a line drawn from the medial tibial spine and the center of the ankle joint.

[2] See discussion on registration and registration free procedure in the conclusion

Fig. 7 Experimental setting: male, 81 (*left*), male, 68 (*right*)

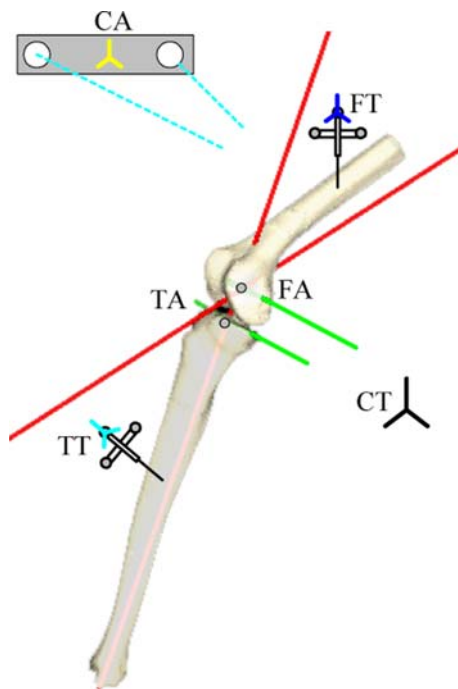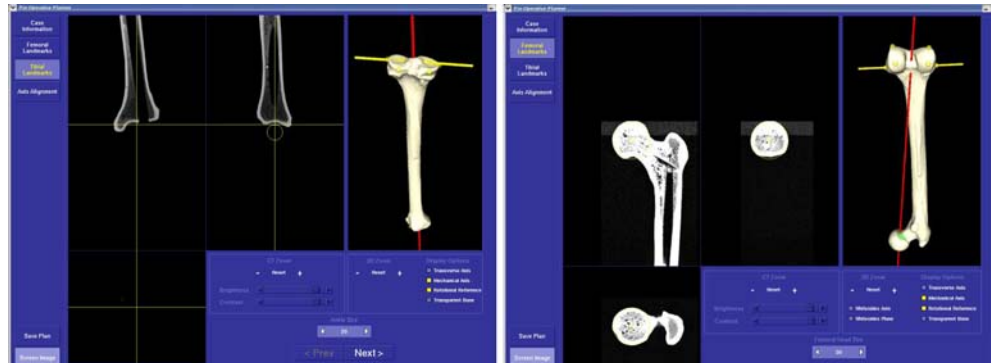**Fig. 8** Tibial ARF (*left*) and Femoral ARF (*right*)

Fig. 9 Tibial, femoral, CT, and camera coordinate systems

During the experiment we obtained $^{FT}T_{TT}$i.e. tibial tracker reference-frame in the femoral tracker reference-frame. We then transformed all data to the anatomical reference system which is the tibial ARF, $^{FA}T_{TA}$, as observed in the femoral reference frame. We obtained $^{FA}T_{TA}$ as

$$^{FA}T_{TA} = {}^{FA}T_{FT} \cdot \underbrace{{}^{FT}T_{TT}}_{observed} \cdot {}^{TT}T_{TA} \tag{10}$$

where

$$^{FA}T_{FT} = \left({}^{CT}T_{FA}\right)^{-1} \cdot \left({}^{FT}T_{CT}\right)^{-1} \tag{11}$$

and finally

$$^{TT}T_{TA} = {}^{TT}T_{CT} \cdot {}^{CT}T_{TA}. \tag{12}$$

Substituting Eqs. (1) and (2) into Eq. (10) we obtain $^{FA}T_{TA}$ as a function of $^{FT}T_{TT}$. Presenting and then analyzing the data in both bones' ARFs allows to repeat this procedure in other patients and therefore analyze data across patients, however, given in the same reference frame.

4 Results

4.1 Sawbones test

A set of results of the Sawbones screw axes is given in Figs. 10 and 11. In Fig. 10 one can see a plot of a single axis given in three views: transverse view (left), coronal view (middle) and a general 3D view of the femur. When the instantaneous screw axes are plotted sequentially, they form a one-parameter rolled surface of lines [18].

Thirty sets of ISP were used for training the SVM classifier, and a different 30 sets were used for testing it. The results of this process are given in Table 1. The columns correspond to the different classes (e.g. healthy, ruptured ACL, etc.) and the rows present the average and standard deviation of the success rate of the classes' identification. Note that the AVG given in the table corresponds to the percentage of the screws per set that were associated with the correct class (averaged on all runs). Referring to Table 1, if we set the threshold for determining a pathology to 82%, we would get 100% success in identification.

While testing these classes, we observed that the main difference between the cases occurred in the last third portion of the flexion–extension motion. This observation suggested that it is sufficient to use the last third portion for the training phase. As a result of this modification, success percentage in some of the classes increased (Table 2). The possibility of gaining increased accuracy by performing the identification and clustering on a subset of the experimental data should be further investigated.

4.2 Cadaver experiment results

It is very difficult to distinguish the differences between the motion of the three knee classes (healthy knee motion, and ACL, ACL + PCL deficient knees) as presented in Fig. 12. However, looking at the instantaneous screw axis it is easier to distinguish the classes. A sample plot of the screw axes of the instantaneous screws for an ACL deficient knee

Table 1 Sawbones experiment: testing all screws in each run (% of correct classification)

	Healthy knee	Ruptured ACL	Ruptured LAT	Ruptured MED	Combination: ruptured MED + ACL
Average	82	99	93	92	87
SD	13.7	1.3	4.4	3.9	6.7

Table 2 Sawbones experiment: testing only last 30% of screws per run (% of correct classification)

	Healthy knee	Ruptured ACL	Ruptured LAT	Ruptured MED	Combination: ruptured MED + ACL
Average	85	99	92	90	90
SD	11.5	0.7	7.0	5.3	11.7

is given in Fig. 13. The resulting plot is a one-parameter rolled surface. Figure 14 is similar to Fig. 13 with an exception that all screw axes of the three classes of one knee are plotted in the same graph. Also plotted in Figs. 13 and 14 (marked with an arrow) is the striction curve of the rolled surface. This curve connects the closest points (distance wise) of two successive screw axes [18]. This curve can also serve as a means to classify kinematic pathologies using curve-fitting techniques; however, we do not use this extra data in this report.

Fig. 10 Screw axis of the first observation: transverse view, coronal view (*middle*) and a 3D view of the femur
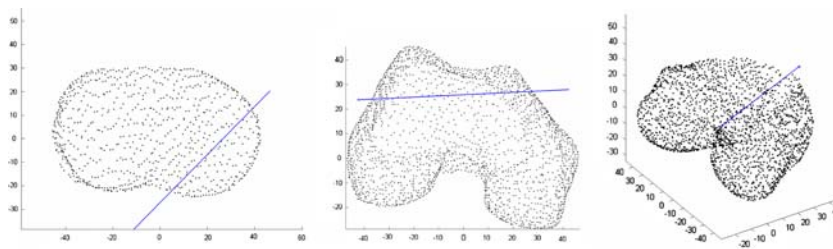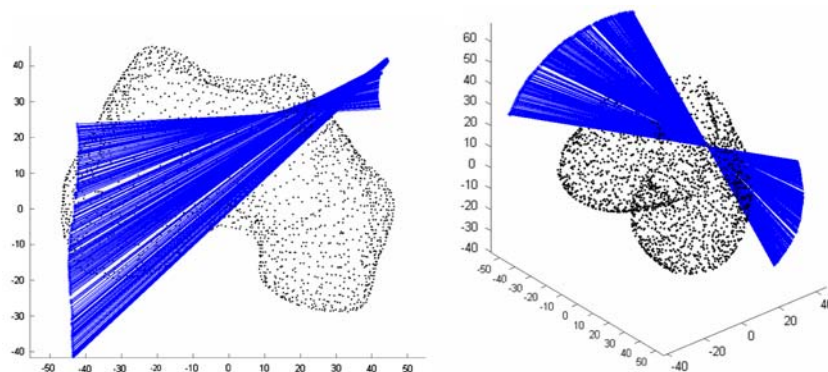

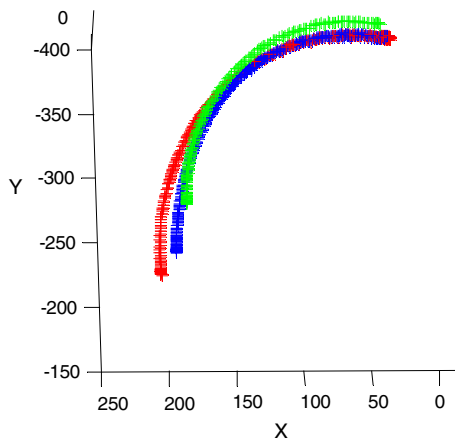**Fig. 11** Screw axis of all observations: coronal view; 3D view

Fig. 12 Tibia tracker origin in femur tracker reference frame (projected onto the sagittal plane) (healthy, ACL, and ACL + PCL deficient)

The results of the SVM classifier are given in Table 3. As can be observed for all classes, the system was able to identify the class with high accuracy. The results of the classifier for a different sampling frequency, i.e. the knee has been manipulated in a different speed resulting in a coarser sampling, are presented in Tables 4 and 5. Since the success rate for the classification process for both cadaver knees across all three pathologies did not decrease substantially, this indicates that sampling frequency does not have to be maintained among experiments (patients).

5 Discussion

In this work we further demonstrate a new method for identifying knee pathologies solely based on kinematics observations. During the experiment we computed the instantaneous screws that describe the knee flexion. These screws were later used for training a classifier to identify
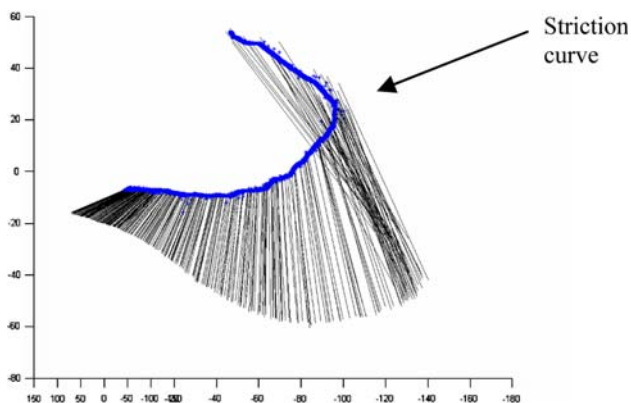

Fig. 13 A views of all the screw axes for ACL deficient knee (knee #2)
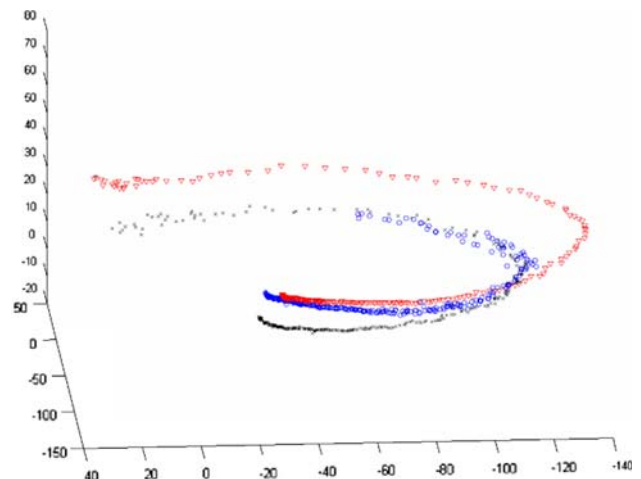

Fig. 14 Striction curves for all three pathologies (knee #2)

different pathologies. The results from both the Sawbones experiment and the two cadaver experiments indicate that it is possible to cluster a set of instantaneous screws which correlates to different knee pathologies, and later use this data to identify knee pathology for a knee never used for training. The classifier was able classify the different

Table 3 Testing all screws in each run: cadaver study (two knees) (sampling full) (true classification %)

	Healthy knee	Ruptured ACL	Combination: ruptured ACL + PCL
Average	77	83	94
SD	4.9	4.7	1.9

Table 4 Testing all screws in each run: cadaver study (two knees) (sampling half) (true classification %)

	Healthy knee	Ruptured ACL	Combination: ruptured ACL + PCL
Average	78	74	96
SD	5.6	9.2	1.6

Table 5 Testing all screws in each run: cadaver study (two knees) (sampling third) (true classification %)

	Healthy knee	Ruptured ACL	Combination: ruptured ACL + PCL
Average	79	74	96
SD	6.6	8.5	2

pathologies with a high success of about 80–90%. We further demonstrate that the capability of the classifier to identify pathologies does not depend on the sampling frequency, i.e. sampling frequency and motion velocity do not have to be synchronized between patients.

In this report we used the SVM algorithm as our classifier. Although this tool has been reported as suitable for biomechanics and gait analysis studies [3], this method has at least one noticeable drawback—the testing method of the classifier. In our SVM classification method, each screw is independently tested against the whole training set while disregarding its relative location in the flexion–extension motion. One possible improvement to explore is to use a different classifier such as the Hidden Markov Model method which will also take into account the sequence and relative location of each instantaneous screw within the set of screws which define the motion, i.e. the system's internal dynamics.

For this report we used a registration procedure in order to define the anatomical reference system of both the tibia and the femur as a global reference systems among patients. One option to simplify this process is to use tracked ultrasound to identify anatomical landmarks which define the anatomical reference system [10]. Another option is to use a parameterized striction curve (Figs. 9, 10) [18]. This curve can then be used by the classifier.

6 Conclusion

To conclude, we introduce a new concept of an expert system which is capable of identifying knee pathologies based on its kinematic observation. The major advantage of the presented method is the use of the ISP to represent the 6-DOF knee kinematics, combined with the use of the SVM classifier. Further investigation should be conducted in order to improve the method; however, the initial results are very promising. It is worth noting that although we report our results for knee kinematics, the same concept can be applied to any other joint or mechanical system of moving rigid bodies.

References

1. Andriacchi T P, Alexander E J., et al. (1998) A point cluster method for in vivo motion analysis: applied to a study of knee kinematics. J Biomech Eng 120(6):743–749
2. Ball RS (1900) A treatise on the theory of screws. Cambridge University Press Cambridge
3. Begg R, Kamruzzaman J (2005) A machine learning approach for automated recognition of movement patterns using basic, kinetic and kinematic gait data. J Biomech 38:401–408
4. Blankevoort L, Huiskes R, et al. (1990) Helical axes of passive knee joint motions. J Biomech 23(12):1219
5. Bottlang M, Marsh JL, et al. (1998) Factors influencing accuracy of screw displacement axis detection with a D.C.-based electro-magnetic tracking system. J Biomech Eng Trans ASME 120(3):431
6. Burges CJC (1998) A tutorial on support vector machines for pattern recognition. Data Mining Knowl Disc 2(2):121–167
7. Caruntu DI, Hefzy MS (2004) 3-D anatomically based dynamic modeling of the human knee to include tibio-femoral and patello-femoral joints. J Biomech Eng 126(1):44–53
8. Davidson JK, Hunt KH (2004) Robots and screw theory: applications of kinematics and statics to robotics. Oxford University Press, New York
9. DiGioia AB, Jaramaz J, et al. (2000) Surgical navigation for total hip replacement with the use of Hipnav. Oper Techn Orthop 10(1):3–8
10. Duck TR, Ferreira LM, et al. (2004) Assessment of screw displacement axis accuracy and repeatability for joint kinematic description using an electromagnetic tracking device. J Biomech 37(1):163
11. Fernandez JW, Hunter P J (2005) An anatomically based patient-specific finite element model of patella articulation: towards a diagnostic tool. Biomech Model Mechanobiol 4(1):20–38
12. Hart R, Mote C J, et al. (1991) A finite helical axis as a landmark for kinematic reference of the knee. J Biomech Eng 113(2):215–222
13. Hasan SS, Hurwitz DE, et al. (1998) Dynamic evaluation of knee instability during gait in anterior cruciate ligament deficient patients. Trans Orthop Res Soc 44:805
14. Hefzy MS, Ebraheim N, Mekhail A, Caruntu D, Lin H, Yeasting R, (2003) Kinematics of the human pelvis following open book injury. Med Eng Phys 25(4):259–274
15. Hunt KH (1978) Kinematic geometry of mechanisms. Clarendon, Oxford
16. Jonsson H, Karrholm J (1994) Three-dimensional knee joint movements during a step-up: evaluation after anterior cruciate ligament rupture. J Orthop Res 12(6):769–779
17. Maki B (1997) Gait changes in older adults: predictors of falls or indicators of fear? J Am Geriatr Soc 45:313–320
18. Pottmann H, Wallner J (2001) Computational line geometry. Springer, Berlin
19. Roth B (1984) Screws, motors, and wrenches that cannot be bought in a hardware store. MIT Press, Cambridge
20. Scholten R J, Opstelten W, et al. (2003) Accuracy of physical diagnostic tests for assessing ruptures of the anterior cruciate ligament: a meta-analysis. J Fam Pract
21. Shiavi R, Limbird T, et al. (1987) Helical motion analysis of the knee—I. Methodology for studying kinematics during locomotion. J Biomech 20:459–469
22. Soudan K, Van Audekercke R, Martens M (1979) Methods, difficulties and inaccuracies in the study of human joint kinematics and pathokinematics by the instant axis concept. Example: the knee joint. J Biomech 12:27–33
23. Vapnik VN (1995) The nature of statistical learning theory. Springer, New York
24. Vapnik VN (1998) Statistical learning theory. Wiley, New York
25. Woltring HJ, Huiskes R, et al. (1985) Finite centroid and helical axis estimation from noisy landmark measurements in the study of human joint kinematics. J Biomech 185:379–389